Water incorporation in synthetic and natural MgAl2O4 spinel

Citation for published version:
Bromiley, GD, Nestola, F, Redfern, SAT & Zhang, M 2010, 'Water incorporation in synthetic and natural MgAl2O4 spinel' Geochimica et Cosmochimica Acta, vol. 74, no. 2, pp. 705-718. DOI: 10.1016/j.gca.2009.10.015

Digital Object Identifier (DOI):
10.1016/j.gca.2009.10.015

Link:
Link to publication record in Edinburgh Research Explorer

Document Version:
Peer reviewed version

Published In:
Geochimica et Cosmochimica Acta

DOI: 10.1016/j.gca.2009.10.015

Water incorporation in synthetic and natural $MgAl_2O_4$ spinel

Geoffrey D. Bromiley*

School of GeoSciences, University of Edinburgh, Grant Institute, West Main Road, Edinburgh EH9 3JW, UK

*Corresponding author. Email: geoffrey.bromiley@ed.ac.uk

Fabrizio Nestola

Dipartimento di Geoscienze, Università di Padova, Via Giotto 1, 35137 Padova (Italy)

Simon A.T. Redfern

Department of Earth Sciences, University of Cambridge, Downing Street, Cambridge CB2 3EQ, UK

Ming Zhang

Department of Earth Sciences, University of Cambridge, Downing Street, Cambridge CB2 3EQ, UK

ABSTRACT

The solubility and incorporation mechanisms of water in synthetic and natural $MgAl_2O_4$ spinel have been investigated in a series of high pressure/temperature annealing experiments. In contrast to most other nominally anhydrous minerals, natural spinel appears to be completely anhydrous. On the other hand, non-stoichiometric Al-rich synthetic (defect) spinel can accommodate several hundred ppm water in the form of structurally-incorporated hydrogen. Infrared (IR) spectra of hydrated defect spinel contain one main O-H stretching band at 3343-3352 cm^{-1} and a doublet consisting of two distinct O-H bands at 3505-3517 cm^{-1} and 3557-3566 cm^{-1}. IR spectra and structural refinements based on single-crystal X-ray data are consistent with hydrogen incorporation in defect spinel onto both octahedral and tetrahedral O-O edges. Fine structure of O-H bands in IR spectra can be explained by partial coupling of interstitial hydrogen with cation vacancies, or by the effects of Mg-Al disorder on the tetrahedral site. The concentration of cation vacancies in defect spinel is a major control on hydrogen affinity. The commercial availability of large single crystals of defect spinel coupled with high water solubility and similarities in water incorporation mechanisms between hydrous defect spinel and hydrous ringwoodite (Mg_2SiO_4) suggests that synthetic defect spinel may be a useful low-pressure analogue material for investigating the causes and consequences of water incorporation in the lower part of Earth's mantle transition zone.

1. INTRODUCTION

Nearly all of the so-called nominally-anhydrous minerals (NAMs) and phases that constitute Earth's mantle can incorporate small but significant amounts of 'water' (Bell and Rossman, 1992; Ingrin and Skogby, 2000). This 'water' is stored as interstitial protons (or hydrogen ions, H^+) bound to specific anion sites in the host structure, characteristically resulting in the formation of spectroscopically active hydroxyl (OH) groups. The water solubility of NAMs in the mantle varies from a few tens, to tens of thousands of parts per million H_2O by weight (ppmw H_2O). As well as constituting a major reservoir of water in the deep Earth interior, the presence of this water has an important, and in some cases dominant, influence on mineral and bulk mantle properties such as melt relations, rheology and electrical conductivity (Mackwell et al., 1985; Gaetani and Grove, 1998; Huang et al., 2005)

Spinels are a class of mineral with the general formula XY_2O_4, in which X and Y can be divalent, trivalent or quadrivalent cations. Oxygen anions in spinel are arranged in a nearly cubic close-packed manner, with X and Y occupying some of the tetrahedral (T) and octahedral (M) interstices in the lattice. Spinel $(Mg,Fe)(Al,Cr)_2O_4$ is a common mineral in the upper mantle, and is the main repository of Al to depths of 50-80 km, at which point it breaks down to form garnet-bearing assemblages. In an ideal (fully ordered) spinel configuration, one-eighth of the T sites and half of the M sites are occupied by X and Y cations respectively, where X = (Mg^{2+}, Fe^{2+}) and Y = (Al^{3+}, Fe^{3+}, Cr^{3+}), hence its description as a 2-3 spinel. In practice, spinel structures are characterized by extensive tetrahedral-octahedral disorder of X and Y cations, especially at elevated temperatures (Redfern et al., 1999; Warren et al., 2000). Despite the importance of spinel, there have been relatively few studies of water incorporation in either natural or synthetic samples, and no investigation of water incorporation under mantle conditions. Most previous studies have focused on characterizing hydrogen and deuterium incorporation in synthetic aluminum-rich non-stoichiometric (defect) spinel ($Mg_{1-x}Al_2O_{4-x}$), and in assessing the usefulness of this material as a proton conductor (e.g. Wang, 1969; Gonzalez et al., 1987; Fukatsu et al., 2002; Okamoto and Maruyama, 2004). There has been no report of hydrogen incorporation in natural spinels (Beran and Libowitzky, 2006), however, and partitioning of water into spinel appears to be very low. Rossman and Smyth (1990) reported that spectroscopic analysis of spinels from high-pressure eclogitic terrains revealed no evidence of hydrogen incorporation, in stark contrast to high water contents noted in other minerals in the same samples. Halmer (2006) reported that detection of OH in Fe-bearing spinel by infrared spectroscopy is hampered by strong absorption over the O-H stretching region due to electronic d-d transitions in tetrahedral Fe^{2+}. In a recent study, Lenaz et al. (2008) concluded that the detection limit of OH in low-Fe spinel samples by infrared spectroscopy should still be around 10-20 ppm H_2O, and noted that their failure to detect OH in low-Fe natural spinel samples implied that water solubility was, at best, extremely limited.

In contrast to $MgAl_2O_4$ spinel, water incorporation in other geologically important spinel group minerals has been extensively investigated. Ringwoodite (Mg_2SiO_4) is a high-pressure polymorph of olivine, and believed to be the most abundant mineral in the lower part of Earth's mantle transition zone. Ringwoodite has been shown to incorporate up to between 1.1 and 2.2 wt% H_2O under mantle transition zone conditions (Kohlstedt et al., 1996; Smyth et al., 2004). OH absorption in Mg_2GeO_4, a low-pressure structural analogue to ringwoodite, has also been investigated (Hertweck and Ingrin, 2005; Thomas et al., 2008).

In order to investigate hydrogen incorporation in spinel, we have performed high-pressure annealing experiments using both natural (low-Fe) and synthetic (defect) $MgAl_2O_4$ spinel. Annealing or synthesizing NAMs under high-pressure high-temperature (high P/T) conditions in hydrous environments greatly increases the amount of 'water' that is incorporated in their crystal structures, due to the strong dependence of water solubility on water fugacity (Lu and Keppler, 1997; Kohlstedt and Mackwell, 1999; Rauch and Keppler, 2002; Bromiley et al., 2004b). Consequently, investigating hydrogen incorporation using infrared spectroscopy is greatly facilitated. Furthermore, hydrogen incorporation in samples that have been equilibrated under realistic mantle conditions provides much better insight into water storage mechanisms in Earth's deep interior, as well as the effects of protonation on mineral properties.

2. EXPERIMENTAL METHODS

2.1 Sample Selection

Two synthetic defect (Al-rich) spinels and one natural, low-Fe spinel were chosen for annealing experiments. Previous work has demonstrated that water solubility in synthetic spinel increases significantly with increase in the amount of excess alumina (Okuyama et al., 2006) and is dependent on sample defect chemistry (Fukatsu et al., 2002; Okuyama et al., 2006). For this reason, we selected two different synthetic spinels with slightly different compositions and grown using different methods. Synthetic spinel 1 was prepared from a large boule of material synthesized via the Verneuil method from a non-stoichiometric mix of high-purity, and came from the same source as sample MgAlVer described by Lenaz et al. (2008). This material was prepared as a doubly-polished 2 mm thick section parallel to (111) and polished down to 1 µm using diamond paste. Spinel 1 has the composition $Mg_{0.4}Al_{2.4}O_{4,}$ unit cell edge length a_0 is 7.9833(4) Å and u = 0.25784(9) (Tables 1 and 2). Analysis of this sample is in excellent agreement with Lenaz et al. and previous workers (Lenaz et al., 2008). Synthetic spinel 2 was purchased from Crystal GmbH as high-purity spinel grown via the Czochralski method. This material was supplied as a doubly-polished 1 mm thick wafer parallel to (111). It has the composition $Mg_{0.4}Al_{2.4}O_{4,}$ unit cell edge length a_0 is 7.9945(4) Å and u = 0.25807(10).

The natural spinel was a low-Fe, Cr-bearing spinel from Myanmar. This material is sourced from alluvial deposits, so its exact origin is unknown. All experiments and measurements were performed using one crystal with an almost perfect octahedral habit and edge lengths of about 4 mm, and a pink coloration (due to the presence of trace amounts of Fe^{2+}). 1 mm thick slabs parallel to (111) were cut from this crystal using a diamond wire saw and polished down to 1 µm using diamond paste. Sample has the composition $MgAl_{1.94}Cr_{0.06}O_4$, unit cell edge length a_0 is 8.1069(7) Å and u = 0.26321(6).

2.2 Microprobe Analysis

Samples were prepared for microprobe analysis by embedding in epoxy and polishing using Si-C paper and diamond solutions down to 0.25 µm. Major element composition of starting materials and selected annealed samples were determined using a Cameca SX100 electron microprobe. Synthetic spinels were analyzed using a 15keV accelerating voltage, 10 nA beam current and highly focused (approx 1µm) beam. For analyzing the natural spinel sample, Mg and Al were analyzed using a 15 keV accelerating voltage and 10 nA beam current and Si, Ca, Ti, Cr, Mn, Fe, Ni and Zn using a 200 nA beam current. Periclase (Mg), corundum (Al), diopside (Si, Ca), rutile (Ti), Cr, Mn, fayalite (Fe), NiO (Ni) and Zn probe standards were used. Compositions of all samples were determined from minimum 30 point analyses. Traverses across starting materials and annealed samples were also taken. No evidence for chemical zonation was found in either synthetic or natural spinel samples or in annealed samples.

2.3 Infrared Spectroscopy

Water contents and hydrogen incorporation mechanisms in spinel samples were determined by Fourier transform infrared spectroscopy (FTIR) from doubly-polished sections of known thickness. Unpolarized mid-infrared (MIR) spectra were obtained using a Bruker IFS-66V spectrometer with a Globar source, KBr beamsplitter, and MCT detector. 512 spectra were obtained for each measurement at a resolution of 2 cm^{-1}. Samples were placed over a 100 µm pin-hole aperture on a sample holder, and the sample holder placed in the internal sample chamber of the spectrometer. The sample chamber was evacuated at high vacuum prior to obtaining spectra to prevent the appearance of anomalous bands due to the presence of water vapor and CO_2. Samples were carefully examined using an optical microscope to ensure that spectra were only obtained from central areas of samples that were crack and inclusion free.

The presence of hydroxyl groups in spinel samples was determined from the presence of characteristic sharp O-H stretching bands in IR spectra over the wavenumber range 4000-2500 cm^{-1}. Because of the lack of mineral specific calibrations for spinel, concentrations of hydroxyl groups were determined using the frequency-dependent calibration of Paterson (1982). In this method the entire infrared absorption spectrum is divided by a frequency dependent extinction coefficient, and the water content determined by numerical integration of the result over the entire frequency range where absorption due to OH bonds is observed. This calibration is derived from measurements of hydroxyl in quartz and silicate glasses, although recent theoretical work by Balan et al. (2008) demonstrates that the Patterson (1982) procedure provides a good calibration for determining hydroxyl concentrations in ringwoodite, which is isostructural with spinel.

2.4 Single-Crystal X-ray Diffraction

Small fragments from each sample between about 200 and 400 μm in size were chosen for the X-ray diffraction study. These fragments were examined optically prior to X-ray measurements to ensure that they were free of twinning and large defects. Unit-cell parameters and full intensity datasets were collected for all samples on a STOE STADI4 four-circle diffractometer (monochromatized $Mo_{K\alpha}$□ radiation) equipped with an Oxford Diffraction CCD detector up to $2\theta_{max} = 85°$ using an exposure time between 10 and 20 s with an ω-scan of 1°. The sample-detector distance was 60 mm. The Crysalis Red program (Oxford Diffraction) was used to integrate the intensity data applying the Lorentz-polarization correction. Absorption correction was performed using X-RED and X-SHAPE software (Stoe and Cie, 1999). For all the samples weighted structural anisotropic refinements were done using SHELX-97 package (Sheldrick, 1997) in $Fd\bar{3}m$ space group (origin at $\bar{3}m$) since no evidence of symmetry deviations was recorded as expected for the compositions investigated. The starting oxygen coordinate of stoichiometric and non-stoichiometric spinels were taken from Lenaz et al. (2008). Refinements were performed using neutral scattering curves for cations whereas a partially ionized curve (O and O^{-2}) was used for oxygen. Crystal data and structure refinement results, together with bond-lengths, polyhedral volumes, and octahedral volume distortion are reported in Table 2. Polyhedral volumes, relative standard deviations and octahedral volume distortion were calculated using IVTON software (Balic-Zunic and Vickovic, 1996).

2.5 Annealing experiments at 1 GPa

Annealing experiments were performed on synthetic spinel 2 using an end-loaded piston-cylinder apparatus. The spinel sample was cut into 1x2x3 mm cuboids using a W wire saw and Si-C slurry. The sample was then soaked in high-purity acetone for several hours and carefully cleaned to remove all traces of slurry. Cuboids of material were placed in 3 mm outer diameter (0.2 mm wall thickness) annealed platinum capsules along with an oxide buffer (with the same composition as the spinel sample) and 10 wt% distilled water. The oxide buffer was made from high purity Al_2O_3 (99.99%) and MgO (99.99%) that had been homogenized by mixing in a ball mill. The purpose of the buffer during annealing experiments was to minimize sample dissolution in, and reaction with, the fluid under high P/T conditions. Platinum capsules were welded shut and carefully weighed, dried and reweighed to ensure they were sealed and that no water had escaped. Capsules were loaded into talc-Pyrex 0.5” piston-cylinder assemblies that contained internal, tapered, graphite resistance heaters of a similar type to those described by (Bromiley et al., 2004b). Capsules were centered in assemblies using MgO spacers and packed in using MgO powder. Capsules were located in the hot spot of assemblies within 1 mm of the thermocouple junction. Piston-cylinder experiments were run using the hot piston in technique; pressure was increased slowly to 90% of the desired final pressure, and then temperature increased at a rate of 100°C/minute to the desired run temperature. Run pressure was then slowly increased to the desired value. Run pressure and temperature were continually monitored and maintain throughout annealing experiments, although in practice, after about 1 hour, pressure stabilized and no longer required correction. Experiments were quenched by shutting off power to heating circuits, and fell to below 300°C after 5 seconds, and to below 100°C after 12 seconds. Experiments were slowly depressurized over 2-3 hours by bleeding off oil pressure using a needle valve to prevent cracking of samples during what is essentially uniaxial decompression. Recovered capsules were pierced, weighed, heated and reweighed to check for the presence of a free fluid phase. Experiments in which there was not strong evidence for the presence of a free fluid phase were discounted. Spinel samples were recovered by carefully opening capsules, drying, and scrapping off the buffer mixture. In all successful runs, a substantial amount of buffer mixture adhered to the samples. Furthermore, all sample surfaces had a milky-white appearance due to reaction and precipitation/recrystallisation. The depth of this reaction zone into the sample was dependent upon annealing time and run temperature. This reaction zone was removed from the two largest faces of the sample by polishing with diamond paste (down to 1 µm), except for one sample in which the reaction front had penetrated the entire thickness of the sample. Formation of this reaction front placed an upper limit of run duration. For spinel experiments described here, maximum run durations that could be achieved were just over 2 days at 1000°C.

Two additional annealing experiments were performed using the natural spinel sample. Due to perceived problems with sample/buffer/fluid reaction and the limited amount of sample material available, run durations of approximately 1 day were used. Experiments were performed using both water and high-purity deuterium oxide (D_2O) fluids.

2.6 Annealing Experiments at 500 bars

In order to perform much longer annealing experiments we performed additional experiments at much lower pressures/temperatures using a hydrothermal bomb apparatus. Synthetic spinel sample 1 was prepared (as above) as polished 2x3x4 mm cuboids, and loaded into welded 4 mm outer diameter, 0.2 mm thick Au capsules with 10 wt% distilled water and a similar oxide buffer mix. Capsules were centered in the hot spot of bombs using SiC rod. Experiments were pressurized to 300 bars water pressure and then slowly heated to 900°C over 2 hours whilst continually bleeding off pressure once it started to exceed the desired final run pressure of 500 bars. Run temperature and pressure were maintained throughout the experiments, and runs were quenched isobarically by first cooling in a rapid air flow and then plunging bombs into water whilst maintaining water pressure. Quench times were 900-500°C over about 20-30s and then 500°C to less than 100°C over about 10s. Recovered capsules were again checked for the presence of a free fluid phase. Recovered annealed crystals showed much less evidence for reaction/recrystallisation, and were again polished down to 1μm for IR examination.

3. RESULTS

3.1 Annealing at 1 GPa

Details of all annealing experiments are listed in Table 3. IR spectra for selected samples are shown in Figures 1-3 and water contents of samples determined from these spectra listed in Table 3. All spectra contain the same features over the wavenumber range 4000 to 2500 cm^{-1} and are similar to spectra obtained from H-bearing defect spinel in previous investigations (Gonzalez et al., 1987; Fukatsu et al., 2002; Okuyama et al., 2006; Lenaz et al., 2008). The two prominent features at approximately 3350 and 3548 cm^{-1} have previously been assigned as two distinct O-H stretching bands on the basis of O-H stretching frequency, dependence of these IR bands on composition and H-D exchange experiments (Gonzalez et al., 1987; Fukatsu et al., 2002; Okuyama et al., 2006). Annealing at 1 GPa results in a considerable increase in water content in the spinel sample, implying H diffusion into the samples under run conditions. Much higher water contents in the annealed samples allow O-H band position to be more accurately determined. Decomposition of spectra (Table 4; see later discussion) demonstrate that IR spectra of defect spinel consist of one O-H band at 3343-49 cm^{-1} (band 1) and an additional doublet, consisting of O-H bands at 3509-3517

cm^{-1} (band 2a) and 3557-3571 cm^{-1} (band 2b). This is most clearly seen by comparing profiles of spectra shown in Figure 3.

Following IR characterization, all samples were prepared for EMP analysis by sectioning using a wire saw, embedding in epoxy and polishing. No evidence for change in major element composition from the starting material or of chemical zonation in the annealed samples was noted (above the detection limits of around 400 ppm for Mg and 600 ppm for Al).

In contrast to the defect spinel, IR spectra from natural spinel annealed at 1 GPa contain no prominent features over the expected O-H stretching range (Figure 2) other than a broad background due to tetrahedrally co-ordinated Fe^{2+} (Lenaz et al., 2008). In comparison, synthetic spinel annealed for around 24 hours under the same conditions contains over 150 ppm H_2O. If the natural spinel sample contains any hydrogen, one would expect that this should be considerably higher than the detection limit possible with FTIR spectroscopy for an Fe-poor sample such as this, which Lenaz et al. (2008) estimate to be around 10 ppmw H_2O. In order to verify this, we performed an additional experiment using D_2O as opposed to H_2O. Gonzalez et al. (1987) demonstrated that hydrogen in defect spinel could be exchanged for deuterium, giving rise to two O-D bands in IR spectra at 2620 and 2480 cm^{-1} (i.e. corresponding to the main OH band and doublet). Absorption due to tetrahedral Fe^{2+} at these wavenumbers is much reduced, which should result in a lower detection limit by FTIR spectroscopy. However, IR spectra for the deuterated natural spinel sample (Figure 2) show no evidence for absorption at these frequencies either. This implies that, in contrast to defect spinel, the natural spinel is essentially completely anhydrous. This observation is in agreement with previous investigations of H incorporation in natural $MgAl_2O_4$-rich spinel (Rossman and Smyth, 1990; Lenaz et al., 2008).

3.2 Annealing at 500 bars

Details of annealing experiments performed at 500 bars (defect spinel 1) are listed in Table 3 along with water contents determined from IR spectra (Figure 3). IR spectra from synthetic spinel 1 annealed at these conditions are very similar to spectra obtained from spinel 2 samples, and consist of a main O-H band (band 1) at 3348-3352 cm^{-1} and a doublet made up of additional O-H bands at 3505-3515 cm^{-1} (2a) and 3555-3557 cm^{-1} (2b). Annealing at lower pressures also results in an initial increase in overall water content, although the amount of water incorporated is much lower compared to experiments performed at 1 GPa. This is consistent with the observed dependence of water solubility in nominally anhydrous conditions on water fugacity, which is itself highly pressure dependent (e.g. Lu and Keppler, 1997; Kohlstedt and Mackwell, 1999; Rauch and Keppler, 2002; Bromiley and Keppler, 2004; Bromiley et al., 2004b). However, with prolonged annealing over approximately 100 hours there is a subsequent decrease in overall water content, as shown in Figure 4. Selected annealed spinel 2 samples were also analyzed by EMP. Once again, we found no evidence for change in major element composition or chemical zonation.

3.3 Structural Refinements

Single-crystal X-ray diffraction data obtained from all three starting materials and one annealed sample were refined to provide detailed information on atomic structure. The natural spinel sample can be directly compared with the natural sample named L-Cr (Olkhon metamorphic complex, Lake Baikal, Russia) studied by Martignago et al. (2003). This sample has practically the same chemical composition and almost identical crystal structure, with *u* coordinate, M-O and T-O distances showing values within one standard deviation with respect to our sample (Table 2). The other three synthetic samples are much richer in Al and, as a consequence of the substitution $3Mg^{2+} = 2Al^{3+} + 1\square$, show a significant content of cation vacancies. For these samples a direct comparison can be made with a non-stoichiometric sample recently studied by Lenaz et al. (2008) and by Nestola et al. (2009b).

X-ray data demonstrate the effect of excess Al_2O_3 and the presence of cation vacancies on crystal structure of spinel. Comparison of stoichiometric and non-stoichiometric samples reveals strong contraction of the unit-cell edge, which decreases from about 8.11 to 7.98 Å in non-stoichiometric spinel. This is mainly due to a reduction in tetrahedral volume of about 15% in non-stoichiometric spinel due to the high-Al content at this site (the Al^{3+} radius in tetrahedral coordination is 0.39 Å compared to 0.57 Å for Mg^{2+}, Shannon, 1976). Conversely, octahedral volume is significantly increased in the non-stoichiometric sample, most likely due to the high proportion of vacant octahedra. However, even if this site were fully occupied one might expect a larger octahedral volume in defect spinel because the natural sample contains both Cr^{3+} and Mg (octahedral Cr^{3+} radius is 0.615 Å, while for Mg^{2+} it is 0.72 Å). The volume of vacant sites is larger than a non-vacant Al site because without a cation present in the gravimetric centre, oxygens are not shielded and mutual repulsion increases site volume. Similarly, there is a significant increase in O-O distance of the shared octahedral edge from the stoichiometric to the non-stoichiometric samples, whilst the O-O distance of the unshared octahedral edge remains almost constant. Finally, the tetrahedral O-O edge decreases significantly from the stoichiometric to the non-stoichiometric samples, again due to increased Al content at the tetrahedral site. A similar structure analysis can be performed among the synthetic non-stoichiometric samples investigated. The annealed and unannealed spinel 1 samples exhibit similar crystal structure features from the unit-cell edge (7.986 and 7.983 Å, respectively) to polyhedral volumes and O-O distances. These two samples show slight but significant differences with respect to spinel sample 2, which has a lower Al content. In particular, the tetrahedral volume is larger for this sample with respect to the other synthetic spinel samples.

4. DISCUSSION

4.1. Stability of defect spinel

As previously noted, defect spinels used in this investigation are non-stoichiometric, Al-rich, and contain high concentrations of cation vacancies. Extensive characterization of defect spinels with varying compositions over the last 50 years has demonstrated that thermal stability is markedly reduced compared to stoichiometric spinel (e.g. Donlon et al., 1982; Saalfeld and Jagodzinski, 1957; Viertel and Seifert, 1979; Wang et al., 1969). At high temperatures, non-stoichiometric spinels precipitate their excess alumina as α-Al_2O_3, resulting in the formation of a stoichiometric spinel host with alumina lamellae. Stability of defect spinel is strongly dependent upon temperature, with more aluminous spinels precipitating alumina at lower temperatures. As such, the possibility of alumina precipitation during high temperature/pressure experiments performed here needs to be considered. Donlon et al. (1982) investigated alumina precipitation in single crystals of defect spinel at temperatures up to 1300˚C and concluded that alumina precipitation in single crystals is suppressed due to the difficulty of nucleation. The most likely cause for suppression is the large strain energy associated with precipitation, which would result in a significant increase in volume. Donlon et al. (1982) concluded that as a result, precipitation of alumina from defect spinel occurs mainly at free surfaces. Optical and SEM examination of prepared, annealed samples in this investigation failed to yield any evidence for alumina precipitation in the bulk of the samples, although the presence of sub-micron-sized lamellae cannot be discounted. It should be noted that precipitation experiments of Donlon et al. (1982) were performed at ambient pressure, and that under the high pressure conditions of annealing experiments outlined here, alumina precipitation should be further suppressed. In contrast, there is abundant evidence for alumina precipitation on the surfaces of annealed defect spinels, especially for samples annealed at higher temperatures (1 GPa experiments). In all runs, a reaction front of varying thickness was observed to penetrate annealed samples. The depth to which this reaction front penetrated the samples was dependent on both run duration and temperature. Depth of penetration of this ‘reaction front’ is consistent with data from Donlon et al. (1982) on the kinetics of alumina precipitation. For example, at 1000˚C, data from Donlon et al. (1982) suggests that a 1mm thick defect spinel should completely recrystallise (i.e. the reaction front should penetrate to the centre of the sample) after 60h annealing time. Likewise, it was noted here that a sample annealed for over 60h at 1.0 GPa/1000˚C had completely recrystallised, compared to a sample annealed for 48h which had only partially recrystallised.

Precipitation of alumina from defect spinel should result in formation of a stoichiometric spinel host. Fukatsu et al. (2002) demonstrated that H solubility in spinel is strongly correlated with the amount of excess alumina. This is consistent with the observation here that annealed natural stoichiometric spinels are entirely anhydrous. One would expect, therefore, that alumina precipitation should result in a marked decrease in H solubility in annealed defect spinel. In all samples annealed at 1 GPa, H solubility increases with annealing time, counter to what would be expected if alumina precipitated in the bulk of the samples. A small decrease in H content was noted in the samples annealed at 500 bars for 163h and 358h. This drop in H solubility could indicate alumina precipitation, although the presence of alumina lamellae was not directly observed, and at the lower run temperatures on the 500 bar experiments, precipitation of alumina/recrystallisation on sample surfaces was minimal.

4.2. Fitting IR spectra

Visual examination of IR spectra obtained from annealed spinel samples strongly suggests that the OH absorption feature at approximately 3550 cm^{-1} is actually a doublet (bands 2a and 2b). To verify this, all spectra were fitted over the entire O-H stretching region using a computer routine (the “Find Peak” routine in the Igor Pro 5.0.3.0 software) that identifies peak maxima by analyzing the first and second order derivatives of the absorption signals. The feature at 3550 cm^{-1} could not be adequately fitted using a single peak profile in any of the spectra, with fitting residues implying the presence of an additional peak (Figure 5). In all cases, spectra could be adequately modeled by 3 Voigt peak profiles and an additional spectral background, with one Voigt peak needed to fit band 1, and 2 Voigt peaks needed to fit band 2 (the feature at 3550 cm^{-1}), supporting the assertion that this band is in fact a doublet (bands 2a and 2b). Results of peak fitting are listed in Table 4, and appear to show a slight increase in the relative height of OH band 1 over the doublet 2a+2b during annealing. However, due to the overlap of bands 2a and 2b, and inherent inaccuracies in band deconvolution, no meaningful trends in relative heights of bands 2a and 2b during prolonged annealing could be determined.

Attempts were made to obtain MIR spectra from annealed samples at liquid N_2 temperature to provide further evidence for the presence of a doublet. However, higher signal/noise ratios from spectra obtained from the small annealed samples held in a cryostat rendered these attempts unsuccessful.

4.3. OH Band Assignment: First possibility

There exists a correlation between O-O distances of protonated polyhedral edges in hydrous and nominally anhydrous minerals and O-H stretching frequencies (i.e. wavenumber of OH bands) in IR spectra (Nakamoto et al., 1955; Libowitzky, 1999). This correlation presupposes that the direction of vibration of OH dipoles is approximately collinear with O-O distances in the host structure, an assumption which holds true for most phases investigated. In a few cases, non-collinear OH vibration can result from strong NNN (next-nearest neighbor) interactions, especially if hydrogen becomes associated with oxygen sites adjacent to cation vacancies, a notable example being the hydrogarnet substitution mechanism (Lager and VonDreele, 1996). However, the recently refined calibration of Libowitzky (1999) can be used, to a first approximation, to find viable docking sites (O-O edges) for hydrogen incorporation using IR data. According to this calibration, IR band 1 can be assigned to protonation of an O-O edge approximately 2.77 Å, band 2a to an O-O edge of 2.91 Å and band 2b to an O-O edge of 3.0 Å. Actual O-O distances in both synthetic spinel crystals and one annealed sample are listed in Table 2. In spinel, there are three distinct O-O distances: a shared octahedral edge, an unshared octahedral edge and a tetrahedral edge. The shared octahedral edge has an O-O distance of approximately 2.6 Å, which appears to be too short to account for O-H bands seen in spinel spectra. By contrast, the unshared octahedral edge is approximately 2.8 Å, and could be a potential site for docking of hydrogen giving rise to OH band 1. IR band 2 can then be assigned to protonation of tetrahedral edges, with a measured O-O distance of 3.0 Å. The observed split of band 2 into a doublet could be the result of some NNN interaction. Lenaz et al. (2008) suggested that IR data for defect spinel are consistent with protonation of O-O edges about vacant tetrahedral sites. Mg^{2+} vacancies on tetrahedral sites would probably result in a slight increase in O-O distances due to increased anion repulsion about the vacant site. Accordingly, splitting of band 2 could be assigned to protonation of O-O edges about both vacant tetrahedral, $V_{Mg}^{//}$ (using the Kröger-Vink notation; Kröger and Vink (1956)), and occupied (Mg) tetrahedra, Mg_{Mg}^{x} . Longer O-O distances about tetrahedral vacancies would result in an increase in O-H stretching frequency, implying that band 2a represents protonation of a normal tetrahedral edge and 2b, protonation of a vacant tetrahedral edge. The concentration of normal (Mg) tetrahedra (Mg_{Mg}^{x}) in spinel samples must be orders of magnitude greater than the concentration of vacant tetrahedral sites ($V_{Mg}^{//}$). The area of band 2b in annealed spinel spectra is of a similar magnitude to that of 2a, implying that protonation of vacant tetrahedral edges is energetically more favourable, as would be expected. Presence of interstitial hydrogen both coupled to substitutional defects (lower valency substitutions) and uncoupled from other defects has been observed in both rutile and stishovite synthesized under high P/T conditions (Bromiley et al., 2004a; Bromiley and Hilaret, 2005; Bromiley and Shiryaev, 2006; Bromiley et al., 2006). Partial defect coupling in rutile and stishovite also results in splitting of OH bands into doublets that may be difficult to resolve at low overall water contents.

Alternatively, splitting of band 2 could be due to protonation of both Mg and Al occupied tetrahedral sites. IR data are consistent with considerable disorder on the tetrahedral site in defect spinel. In this instance, the presence of Al on T sites ($Al_{Mg}^{\cdots}$) results in contraction of the site, and a decrease in O-O edge distance. This would imply that band 2a was due to protonation of the O-O tetrahedral $Al_{Mg}^{\cdot}$ edge, and band 2b to protonation of the O-O tetrahedral Mg_{Mg}^{x} edge.

4.4 OH band Assignment: Second possibility

Protonation of vacant cation sites has been proposed as a dominant mechanism for hydrogen incorporation in a number of nominally anhydrous minerals (Smyth et al., 1991; Lager and VonDreele, 1996; Smyth et al., 2003; Smyth et al., 2006). X-ray data for synthetic defect spinel are consistent with a high concentration of cation vacancies on the octahedral site ($V_{Al}^{///}$). Protonation of such sites would appear highly favorable, due to the strong net negative charge associated with a cation vacancy. On this basis, an alternative assignment of OH bands in spinel spectra can be suggested. Structural refinements of X-ray data from this study demonstrate that the presence of high concentrations of octahedral vacancies in defect spinel results in a significant overall increase in octahedral volume. The presence of $V_{Al}^{///}$ is expected to result in significant increases in O-O distances about the vacant site. Assuming O-H bond co-linearity with O-O octahedral edges, OH band 1 can be assigned to protonation of the shared octahedral O-O edge about a vacant octahedral site if there is an increase in O-O distance of slightly less than 5%. This is consistent with the difference in O-O distance between stoichiometric (natural) and non-stoichiometric spinel listed in Table 2. This assignment also holds if there is minimal overall change in O-O distances but a significant deviation in O-H bond vibration away from the O-O direction. Extending this argument, OH band 2a can then be assigned to protonation of the unshared octahedral O-O edge; in this instance, an increase in actual O-O distance of about 3% is required to account for the observed O-H stretching frequency. X-ray data (Table 2) imply that the unshared octahedral edge in defect spinel is actually shorter than in stoichiometric spinel. However, differences in calculated and actual O-O distances for this band could again be due to non-linearity of O-H bands with specific O-O edges. Band 2b can then be assigned to protonation of a tetrahredral edge in this scheme.

Protonation of both shared and unshared octahedral edges could provide partial local charge compensation associated with $V_{Al}^{///}$, although the assignment is not dependent on the formation of OH pairs about vacant sites. In fact, Fukatsu et al. (2002) demonstrated that water (hydroxyl) solubility in defect spinel is proportional to the half power of the partial pressure of water, implying that hydrogen is incorporated into the structure as isolated OH^- defects, and not as pairs or clusters of OH^-.

Assignments 1 and 2 both imply protonation of octahedral and tetrahedral edges and imply that defect coupling must be important under high P/T conditions. Many previous studies have highlighted the rapid kinetics of Mg-Al order/disorder at high T and high P/T in spinel (e.g. Redfern et al., 1999; Meducin et al., 2004), and that fact that high degrees of disorder in spinel at temperatures around 1000°C cannot be quenched, with samples becoming more ordered even during rapid quenching. However, the degree of ordering in spinel, and changes in degree of ordering, appear to be strongly dependent on composition. Recent investigations of high T and high P behavior of defect spinel demonstrate that oxygen coordinate remains almost constant as a function of pressure or temperature (Nestola et al., 2009a,b). Since the oxygen coordinate varies strongly with degree of order, this suggests that no significant change in order occurs in the defect samples during high T annealing. This is also demonstrated by comparing relative OH band heights between samples annealed at 1273 K and 1573 K at 1 GPa (Figure 1). No significant differences are noted between spectra annealed under these different conditions. Investigation of hydrogen incorporation in $MgSiO_3$ enstatite demonstrates that changes in crystal structure that occur during quenching (in this example, the high-pressure clinoenstatite, C2/*c*, to low-clinoenstatite, $P2_1/c$, martensitic phase transformation) result in identifiable signatures in topology of O-H stretching bands in IR spectra (Bromiley and Bromiley, 2006). Any major change in degree of disorder in the spinel samples during annealing/hydration would be expected, on this basis, to result in changes in relative OH band height and/or position. This implies that patterns in the distribution of hydrogen between different O-O sites observed in spectra obtained from annealed samples at room temperature closely resemble those under high P/T conditions of the annealing experiments.

4.5 Diffusion of Species During Annealing

Hydrogen incorporation in defect spinel requires some charge balancing mechanism. X-ray data are consistent with a large concentration of octahedral (Al) vacancies in the samples. The major mechanism for incorporating excess Al_2O_3 in defect spinel, on the basis of X-ray refinements, is likely to be a Schottky substitution of Al for divalent Mg cations balanced by the formation of cation vacancies on octahedral sites (Mitchell, 1999):

$$4Al_2O_3 \rightarrow 3Al_{Mg}^{\cdot} + V_{Al}^{///} + 5Al_{Al}^{x} + 12O_{O}^{x} \qquad [1]$$

Alternatively, cation vacancies can form on the tetrahedral sites (Mitchell, 1999):

$$4Al_2O_3 \rightarrow 6Al_{Al}^{x} + 2Al_{Mg}^{\cdot} + V_{Mg}^{//} + 12O_{O}^{x} \qquad [2]$$

In either case, the concentration of cation vacancies is the same and no oxygen vacancies are present. However, Fukatsu et al. (2002) noted that experimental results on the dependence of self-diffusion of oxygen on Al_2O_3 content of spinel imply that Al-rich spinels contain more oxygen vacancies compared to stoichiometric samples.

Hydrogen incorporation in spinel could also be charge-balanced by cation vacancies on either tetrahedral or octahedral sites:

$$Mg_{Mg}^{x} + H_2O \longrightarrow V_{Mg}^{//} + 2H_i^{\bullet} + MgO \qquad [3]$$

$$2Al_{Al}^{x} + 3H_2O \longrightarrow 2V_{Al}^{///} + 6H_i^{\bullet} + Al_2O_3 \qquad [4]$$

This could explain hydrogen incorporation in the synthetic starting materials, assuming that protonation occurred during synthesis. During annealing experiments, prolonged hydration of samples requires charge-balancing by counter diffusion of another positively charged species. For diffusion studies of most NAMs, this is usually counter diffusion of polarons, i.e. a change in the valence of Fe^{3+} to Fe^{2+} (Mackwell and Kohlstedt, 1990; Skogby, 1994; Bromiley et al., 2004b), although this cannot be the case with our synthetic spinel. Instead, diffusion of hydrogen into the spinel samples must be compensated by diffusion of Mg^{2+}, Al^{3+} or oxygen vacancies out of the samples.

Diffusivity of hydrogen in spinel was determined by Gonzalez et al. (1987) and Fukatsu et al. (2002) via hydrogen-deuterium exchange experiments and hydrogen uptake/loss experiments, respectively. Results from these studies are consistent, although data, strictly speaking, only concern the OH band at 3350 cm^{-1}. Extrapolating diffusion coefficients for hydrogen in defect spinel to 1273 K (and assuming a negligible effect of pressure), annealing for 48 hours would result in diffusion of hydrogen to a depth of 0.2 mm. This is consistent with piston-cylinder experiments, in which no evidence for saturation of hydrogen was found in the 1 mm thick samples after annealing up to 2 days. Extrapolating diffusion data to 1173 K introduces a large uncertainty, but implies that the 1 mm spinel sample should contain an equilibrium OH content (at least for OH band 1) after 300 hours. In fact, water solubility in the spinel samples annealed at 1173 K/500 bars shows a more complex relationship with annealing time, and initially (up to about 100 hours) increases and then decreases. However, general trends seen in spinel hydration experiments are consistent with hydrogen diffusion into the samples. Diffusion of hydrogen into the spinel samples could either be coupled with diffusion of oxygen into the samples (diffusion of anion vacancies):

$$V_O^{\bullet\bullet} + H_2O \longrightarrow 2H_i^{\bullet} + O_O^x \qquad [5]$$

or diffusion of Mg or Al out of the samples (equations [3] and [4], respectively).There is only limited data on diffusion of these species in spinel (Reddy and Cooper, 1981; Liermann and Ganguly, 2002). In single crystal hydration/dehydration studies, Fukatsu et al. (2002) concluded that hydrogen diffusion must be coupled to diffusion of $V_O^{\cdot\cdot}$, due to a lack of evidence for MgO or Al_2O_3 precipitation on crystal surfaces. Comparable results on hydrogen diffusivity between this study and the work of Fukatsu et al. (2002) suggest that hydrogen diffusion coupled to oxygen vacancy diffusion is an appropriate model. If correct, this implies that the concentration of $V_O^{\cdot\cdot}$ in the starting material may be the most important factor controlling hydrogen affinity during the annealing experiments. As well as charge-balancing hydrogen diffusion, diffusion of oxygen into the samples would result in an increase in hydrogen affinity due to a decrease in anion overbonding and increase in number of potential hydrogen docking sites. Long duration annealing experiments, however, show a decrease in water content in runs over approximately 100 hours, similar to that reported in long duration hydration experiments on synthetic orthopyroxene (Stalder and Skogby, 2003). Results appear to suggest that slower diffusion of some additional species occurs in long duration experiments. This could be explained by either Mg^{2+} or Al^{2+} diffusion into the samples. Alternatively (as noted above), precipitation of alumina from the bulk of the defect spinel crystals during prolonged annealing would also result in a decrease in water content, although there is no direct evidence to support alumina precipitation in the bulk of any of the samples.

5. HYDROGEN INCORPORATION IN SPINEL-TYPE PHASES IN EARTH'S MANTLE

Results from this study and previous studies suggest that $MgAl_2O_4$ spinel can, at best, only contain relatively insignificant amounts of water as structurally-incorporated hydrogen under conditions of the top of Earth's mantle. Hydrogen incorporation in spinel is probably strongly dependent on non-stoichiometry and concentration of cation (octahedral) vacancies. However, hydrogen incorporation in other mantle phases with spinel-type structures is likely to be extremely important. Ringwoodite (Mg_2SiO_4) is the major phase present in the lower part of the mantle transition zone. This 4-2 normal spinel can incorporate significant amounts of water. Smyth et al. (2003) demonstrated that hydration of ringwoodite is strongly correlated with the number of Mg (octahedral) vacancies, with close to full occupancy of tetrahedral (Si) sites. Smyth et al. (2003) also noted that the main OH band in IR spectra from ringwoodite is consistent with protonation of tetrahedral edges, although there is additional evidence for protonation of octahedral edges in some ringwoodite samples (Kohlstedt et al., 1996; Kudoh et al., 2000; Smyth et al., 2003). There are, therefore, many similarities in hydrogen incorporation between ringwoodite and spinel, most notably protonation of both octahedral and tetrahedral edges charge-balanced by octahedral vacancies. Interestingly, protonation of tetrahedral edges appears more favorable in the ringwoodite structure, with protonation of octahedral edges only observed in very hydrous samples. The opposite is noted in spinel. Gonzalez et al. (1987) report that IR spectra from nominally stoichiometric spinel only contain absorption band 1, which is assigned to protonation of the octahedral edge. This is most likely due to preferential protonation of this edge in samples with inherently low water solubility (i.e. very low concentrations of cation vacancies). This difference may relate to the relative size of octahedral and tetrahedral sites in the two structures, and the charge of the coordinating cation. For hydrogen incorporation about vacant cation sites, protonation of vacant tetrahedra ($V_{Si}^{////}$) in ringwoodite and octahedral in spinel ($V_{Al}^{///}$) would appear more likely. Likewise, the tetrahedral edge is the shortest O-O distance in ringwoodite, but the longest O-O distance in spinel.

Hertweck and Ingrin (2005) investigated hydrogen incorporation in the 4-2 spinel Mg_2GeO_4, a low-pressure structural analogue of ringwoodite. IR spectra obtained from this phase contained one main OH band at 3531 cm^{-1} with a shoulder at 3502 cm^{-1}, which Hertweck and Ingrin (2005) assigned to protonation of the tetrahedral edge, consistent with investigations of ringwoodite. O-H stretching frequencies for the two bands in Mg_2GeO_4 spectra correspond to O-O distances of 2.95 and 2.90 Å. Actual O-O distances in Mg_2GeO_4 are 2.935 Å for the tetrahedral edge, 2.935 Å for the shared octahedral edge and 2.917 Å for the unshared octahedral edge. O-H bands could, therefore, just as easily be assigned to protonation of both tetrahedral and octahedral edges.

Similarities in hydrogen incorporation in both defect spinel and ringwoodite suggest that defect spinel is a useful low-pressure analogue for investigating the causes and consequences of hydrogen incorporation in ringwoodite. Water solubility in defect spinel is likely to depend on both composition (Fukatsu et al., 2002) and defect chemistry of samples. In the present study, we note water contents as high as 371 ppmw H_2O for defect spinel annealed at 1 GPa, 1573 K for 5 hours. This value probably does not represent saturation of the sample with hydrogen, and is a lower estimate for water solubility. However, solubility of water in defect spinel at these conditions is considerably higher than many other NAMs (Keppler and Bolfan-Casanova, 2008). Dependence of hydroxyl content on the square root of water fugacity (Fukatsu et al., 2002) implies that annealing spinel at higher pressures should result in even higher water contents. High-pressure annealing of large (mm sized) defect spinel under hydrous conditions should provide a useful material for investigating properties of a wet mantle transition zone

Acknowledgements

Experimental work was performed at the Dept, Earth Sciences, University of Cambridge, and was supported by NERC grant LBZF/039. GDB acknowledges the support of the Leverhulme Trust. The authors thank Paul Taylor for help with hydrothermal bomb experiments. This manuscript was greatly improved by the constructive reviews of Roland Stalder, Anton Beran and an anonymous reviewer.

Table 1. Compositions of spinel starting materials and selected annealed samples (details given in Table 3) determined by EMPA. Data are averaged from 30+ point analyses. Figures in parentheses are 2σ errors on mean values.

	Synthetic spinel 1	Synthetic spinel 2	Natural Cr-spinel	1 GPa, 1273K, 48h	0.05 GPa, 1173K, 163h
MgO	11.61(52)	13.06(8)	27.88(15)	13.16(13)	11.33(41)
Al_2O_3	87.99(52)	86.64(8)	67.43(55)	85.99(29)	87.81(44)
SiO_2			0.02(0)		
CaO			0.01(0)		
TiO_2			0.09(2)		
Cr_2O_3			3.23(59)		
FeO			0.05(1)		
ZnO			0.05(3)		
Total	99.6(9)	99.7(5)	98.79	99.2(3)	99.1(4)

Table 2. Results of structure refinement and cation distribution of the investigated spinels.

Sample	**Natural spinel**	**Synthetic spinel 1**	**Spinel 1 annealed at 0.05 GPa, 1173 K for 163 hours**[1]	**Synthetic spinel 2**
a_0 (Å)	8.1069(7)	7.9833(5)	7.9860(5)	7.9945(4)
V (Å^3)	532.80	508.80	509.32	510.94
u	0.26321(6)	0.25784(9)	0.25781(7)	0.25807(10)
M-O (Å)	1.9256(4)	1.9352(7)	1.9361(5)	1.9363(7)
T-O (Å)	1.9407(8)	1.8369(13)	1.8370(10)	1.8425(14)
V_M (Å^3)	9.347(5)	9.608(7)	9.618(5)	9.615(7)

V_T (Å^3)	3.751(2)	3.179(3)	3.182(2)	3.211(3)
^{VI}O – O	2.563(1)	2.645(2)	2.647(2)	2.644(2)
^{IV}O–O	3.169(1)	3.000(2)	3.000(2)	3.009(2)
^{VI}O–O_{unsh}	2.8742(3)	2.8253(2)	2.8262(2)	2.8294(2)
U(M) (Å^2×10^{-4})	0.0041(1)	0.0086(3)	0.0080(2)	0.0091(3)
U(T) (Å^2×10^{-4})	0.0054(2)	0.0057(3)	0.0050(2)	0.0065(3)
U(O) (Å^2×10^{-4})	0.0058(2)	0.0114(3)	0.0125(2)	0.0121(5)
N. refl.	118	113	109	106
R_1	1.1	2.8	2.0	3.5
wR^2	1.7	8.1	4.5	7.9
GooF	0.9	1.1	1.0	1.1
2θ_{max}(°)	85	85	85	85
Cation distribution				
T site				
Mg	0.85	0.40	0.45	0.40
Al	0.15	0.60	0.55	0.60
M site				
Mg	0.15	-	-	-
Al	1.79	1.80	1.82	1.80
Cr	0.06	-		-
Vacancies	-	0.20	0.18	0.20
Sum	3.00	3.00	3.00	3.00

[1]See Table 3 for experimental conditions

Table 3. Experimental conditions for natural and synthetic spinel hydrogenation and deuteration experiments and water contents determined from IR absorption.

Pressure (GPa)[1]	**Temperature (K)**	**Duration (h)**	**Notes**	**Concentration OH (ppmw H_2O)**
Experiments using synthetic spinel 1				
-	-	-	starting material	58
0.05	1173	24		69
0.05	1173	48		73
0.05	1173	70		79
0.05	1173	163		76
0.05	1173	358		65
Experiments using synthetic spinel 2				
-	-	-	starting material	10
1.0	1273	10		83
1.0	1273	17		128
1.0	1273	48		342
1.0	1273	66.5	sample completely recrystallized	not analyzed
1.0	1573	5		371
Experiments using natural spinel				
-	-	-	starting material	0
1.0	1173	21	hydration experiment	not detected
1.0	1173	24	deuteration experiment	not detected

[1]Experiments at 0.05 GPa performed using hydrothermal bomb apparatus, and experiments at 1 GPa using piston-cylinder apparatus.

Table 4. Results of OH band fitting of MIR spectra. Spectra were fitted as 3 Voigt profiles (with an additional background). Numbers in parentheses are standard deviations.

	Band 1						Band 2a						Band 2b					
	Pos (cm^{-1})	Area (cm^{-2})	Width (cm^{-1})	Gauss width (cm^{-1})	Lor width (cm^{-1})	shape	Pos (cm^{-1})	Area (cm^{-2})	Width (cm^{-1})	Gauss width (cm^{-1})	Lor width (cm^{-1})	shape	Pos (cm^{-1})	Area (cm^{-2})	Width (cm^{-1})	Gauss width (cm^{-1})	Lor width (cm^{-1})	shape
Annealing experiments at 0.05 GPa																		
SM	3351.6(0)	319.2(8)	109.5	28.9(9)	101.9(5)	2.9(1)	3505.1(8)	43.2(19)	67.9	67.9(12)	0.0(5)	0.0(0)	3557.2(11)	76.0(20)	80.6	34.4(30)	65.9(19)	1.6(2)
24h	3351.1(1)	428.6(17)	103.3	27.9(13)	95.7(7)	2.9(2)	3506.6(13)	39.6(27)	59.5	59.3(32)	0.4(4)	0.0(0)	3555.2(14)	84.5(30)	71.1	30.1(45)	58.4(28)	1.6(3)
48h	3348.4(1)	450.7(32)	115.3	27.0(28)	109.0(13)	3.4(4)	3510.7(21)	33.1(35)	57.3	57.2(59)	0.1(7)	0.0(1)	3557.1(21)	58.6(38)	61.4	30.7(66)	46.1(51)	1.2(4)
70h	3349.3(1)	486.9(30)	110.0	27.5(22)	103.1(12)	3.1(3)	3510.0(18)	38.6(37)	57.4	57.3(47)	0.1(6)	0.0(1)	3556.5(20)	74.6(4)	64.1	29.3(61)	50.7(42)	1.4(4)
163h	3349.2(1)	417.6(27)	110.0	27.8(23)	102.9(12)	3.1(3)	3510.8(20)	29.1(33)	55.4	55.4(53)	0.1(7)	0.0(1)	3556.8(21)	62.1(37)	63.7	29.7(66)	49.8(4)	1.4(4)
358h	3349.0(1)	444.5(32)	109.5	28.3(26)	102.2(14)	3.0(3)	3515.6(26)	31.6(38)	58.0	57.4(69)	1.1(8)	0.0(1)	3561.0(25)	50.9(42)	59.5	30.1(77)	44.2(63)	1.2(5)
Annealing experiments at 1.0 GPa																		
SM[1]	3348.1(7)	58.0(11)	151.3	47.6(8)	136.3(24)	2.4(0)	3509.2(90)	9.0(40)	70.5	70.5(15)	0.1(0)	0.0(0)	3566.3(10)	5.4(18)	71.0	30.9(42)	57.5(15)	1.5(3)
10h	3343.7(5)	919.4(12)	198.9	49.5(71)	186.5(38)	3.1(5)	3517.1(33)	79.9(93)	73.8	73.7(10)	0.43(15)	0.0(1)	3571.2(43)	88.6(95)	74.6	39.8(11)	53.4(10)	1.1(5)
17h	3347.3(2)	785.1(66)	139.0	40.7(34)	127.1(21)	2.6(3)	3510.0	76.5(11)	66.2	66.2(40)	0.0(1)	0.0(0)	3561.9(38)	97(11)	71.1	50.7(77)	35.0(6)	0.6(2)
48h	3348.5(1)	2200.4(11)	120.1	29.9(22)	112.7(11)	3.1(3)	3513.5(16)	228.4(16)	66.3	66.3(23)	0.0(5)	0.0(0)	3561.9(18)	290.3(18)	66.9	31.3(58)	52.3(43)	1.4(4)
5h at 1573K	3348.3(1)	2401.6(12)	125.3	32.4(21)	116.9(11)	3.0(2)	3509.2(17)	210.6(19)	61.2	61.2(24)	0.0(4)	0.0(0)	3557.0(18)	401.9(21)	70.4	30.9(54)	56.9(35)	1.5(4)

SM=starting material used for each sequence of experiments (synthetic spinels 1 and 2, respectively), *Pos*=fitted IR band position, *Gauss*=Gaussian component, *Lor*=Lorentzian component

[1]Accuracy of peak fitting for spinel 1 starting material is much poorer due to poor signal/noise ratio for this spectrum.

FIGURES

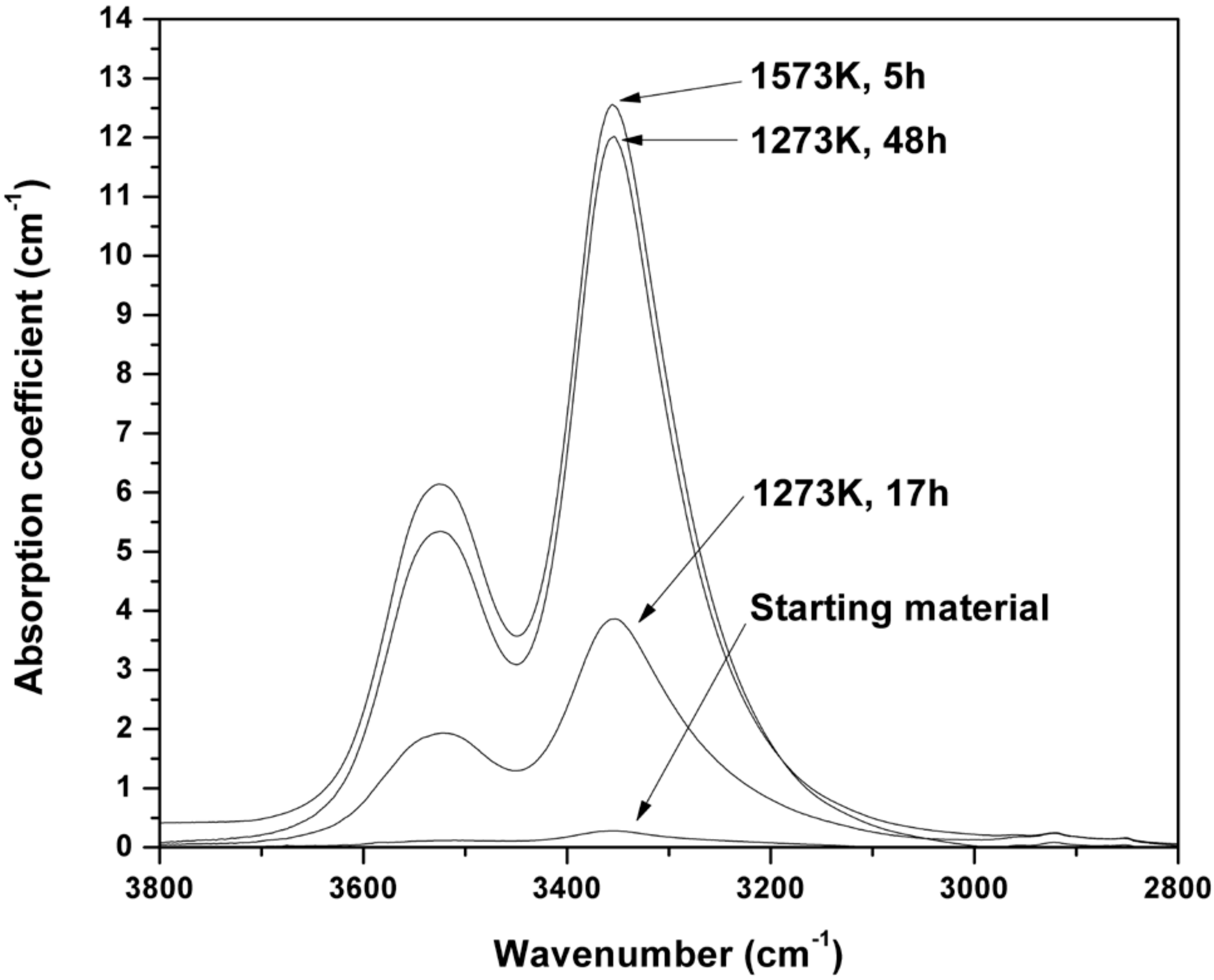

Figure 1. Unpolarized IR spectra from synthetic defect spinel 1 before and after annealing at 1 GPa under hydrous conditions (not all spectra shown for clarity). Spectra are background corrected and normalized.

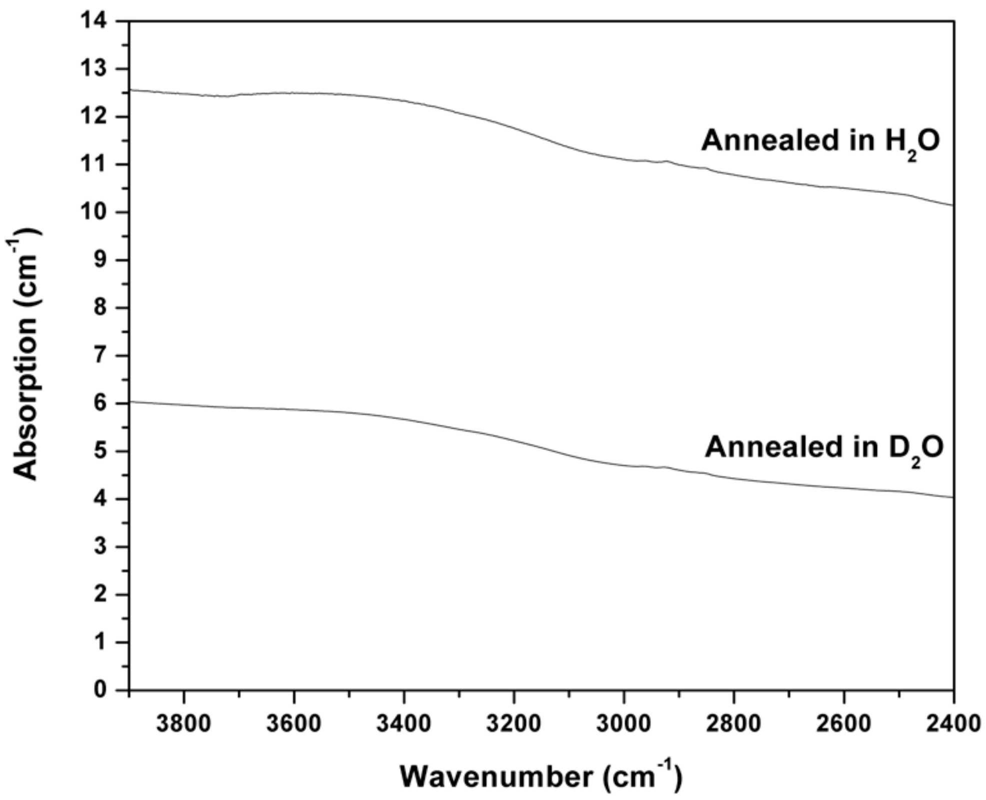

Figure 2. Unpolarized IR spectra from natural Cr-spinel annealed at 1 GPa, 1273K (no background correction).

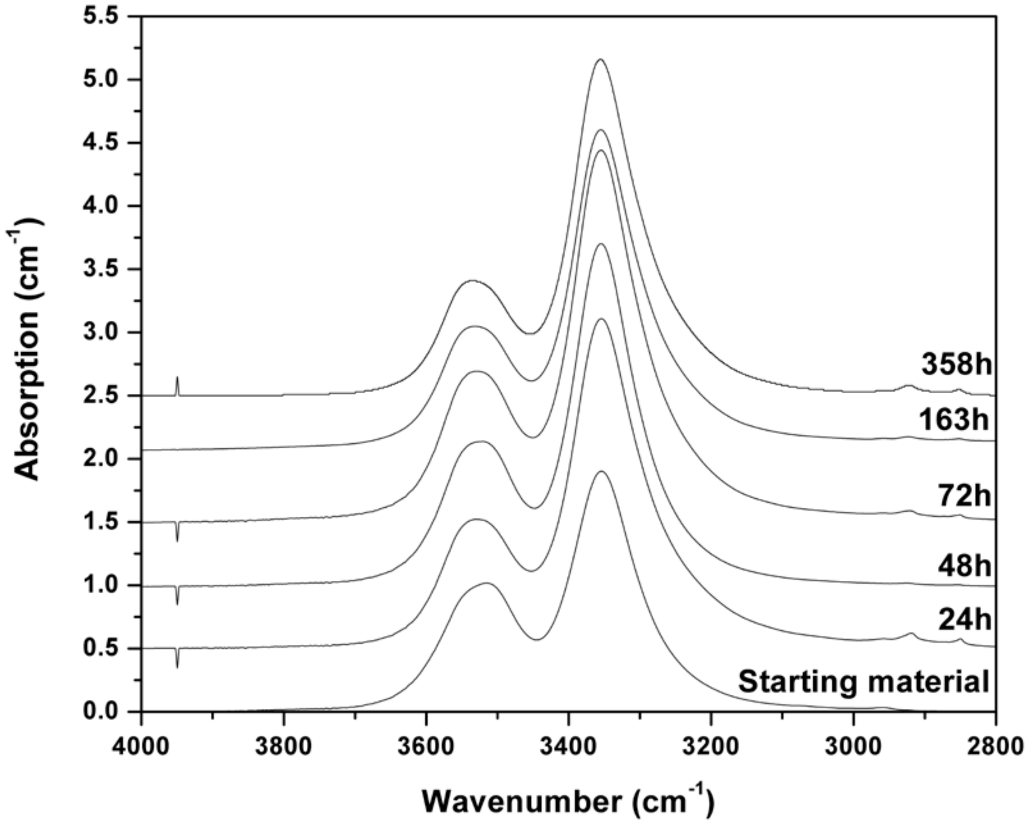

Figure 3. Unpolarized IR spectra from synthetic defect spinel 1 before and after annealing at 0.05 GPa, 1173K under hydrous conditions. Spectra are background corrected and normalised and offset vertically (with increasing annealing time) for clarity.

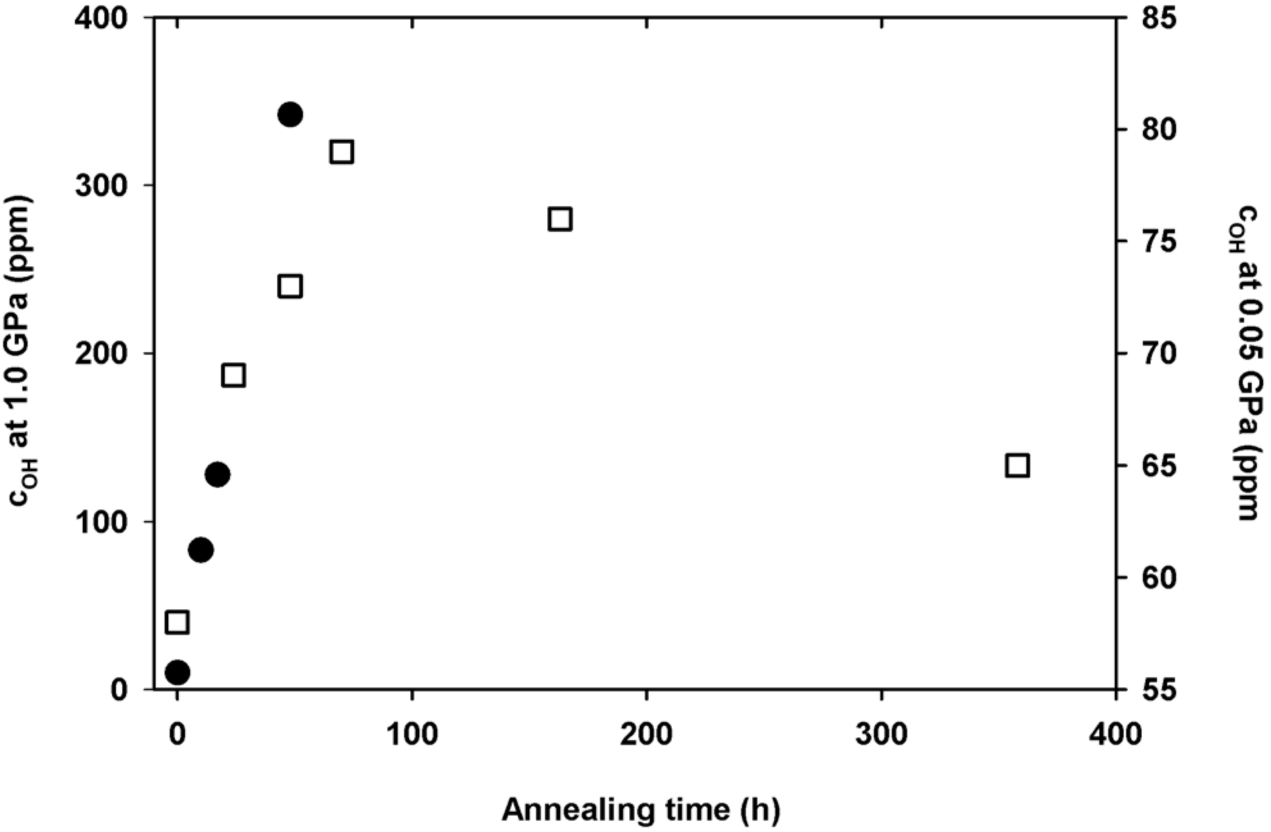

Figure 4. Plot of concentration of OH (expressed as ppm H_2O by weight) in defect spinel annealed at 1 GPa (filled circles, left hand scale) and 0.05 GPa (open squares, right-hand scale) as a function of annealing time.

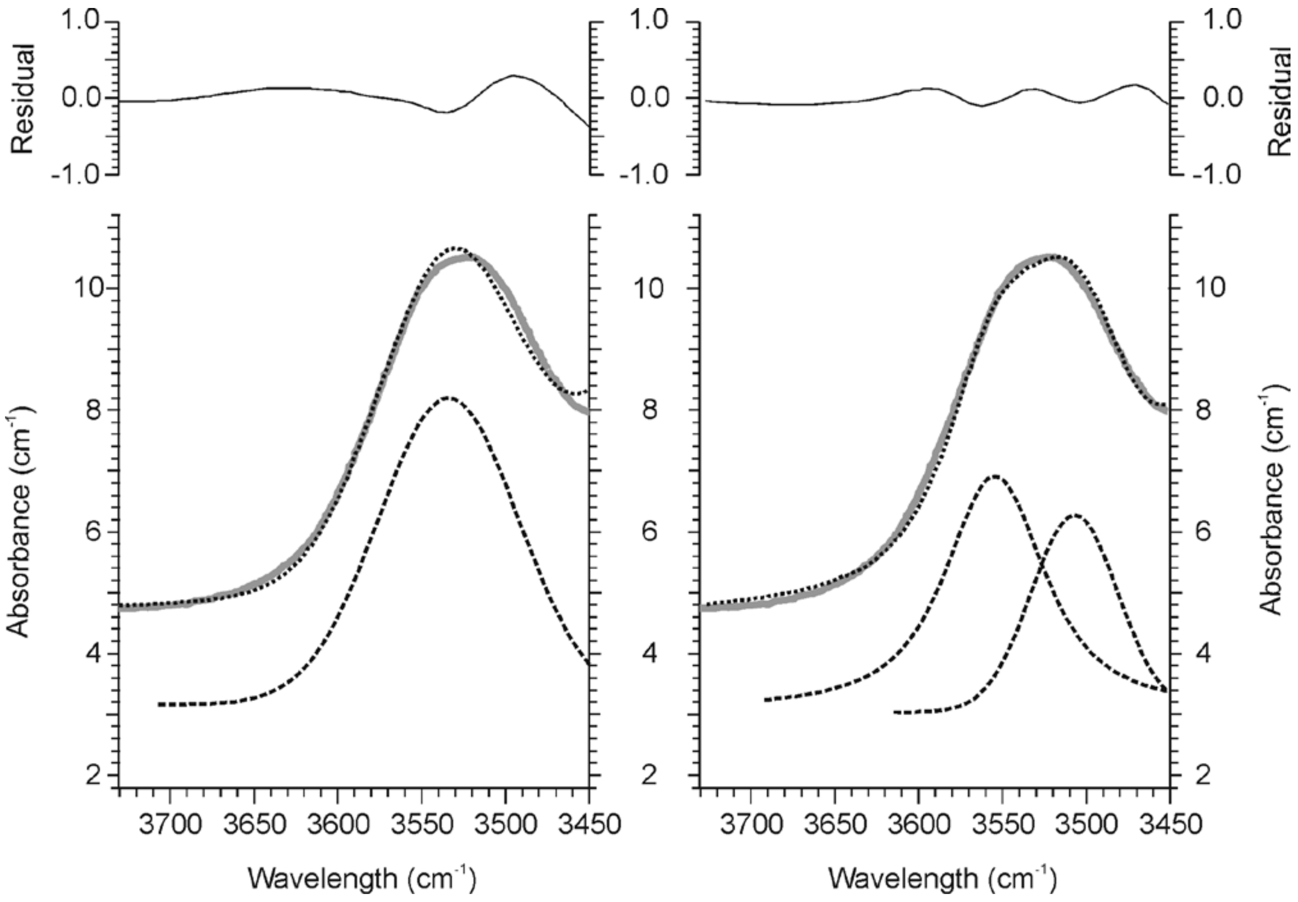

Figure 5. An example of band deconvolution of the O-H absorption feature at 3500-3550 cm^{-1} using Igor Pro, fitted as either one (left) or 2 (right) Voigt peaks. The thick grey line is the recorded spectra and the fine dotted line the fit to the data (using peak profiles shown at the bottom as dashed lines). Residues from the fitting are shown at the top of the figure. This absorption feature could not be adequately modeled as one single band, as evident from the large ‘peak’ in the fit residue. A much better fit is obtained using 2 separate Voigt peak profiles, supporting the assertion that this feature is in fact a doublet (band 2a at 3505-3517 cm^{-1} and band 2b at 3557-3571 cm^{-1})

REFERENCES

Balan E., Refson K.,Blanchard M.,Delattre S., Lazzeri M., Ingrin J., Mauri F., Wright K., and Winkler B. Theoretical infrared absorption coefficient of OH groups in minerals. *Am. Mineral.* **93**, 950-953

Balic-Zunic T., and Vickovic I. (1996) IVTON -a program for the calculation of geometrical aspects of crystal structures and some crystal chemical applications. *J. App. Crys.* **29**, 305-306.

Bell D., and Rossman G. (1992) Water in Earth's Mantle. The role of nominally anhydrous minerals. *Science* **255**, 1391-1397.

Beran A. and Libowitzky E (2006) Water in natural mantle minerals II: Olivine, garnet and accessory minerals. *Rev. Mineral. Geochem.* **62**, 169-191.

Bromiley G. and Keppler H. (2004) An experimental investigation of hydroxyl solubility in jadeite and Na-rich pyroxenes. *Contrib. Mineral. Petrol.* **147**, 189-200.

Bromiley G. and Hilaret N. (2005) An investigation of hydrogen and minor element incorporation in synthetic rutile. *Mineral. Mag.* **69** (3), 345-358.

Bromiley G. and Bromiley F. (2006) High-pressure phase transitions and hydrogen incorporation in $MgSiO_3$ enstatite. *Am. Mineral* **91**, 1094-1101.

Bromiley G., and Shiryaev A.A. (2006) Neutron irradiation and post-irradiation annealing of rutile (TiO_2-x): effects on hydrogen incorporation and optical absorption. *Phys. Chem. Minerals* **33** (6), 426-434.

Bromiley G., Bromiley D., and Bromiley F. (2006) On the mechanisms for aluminum and hydrogen incorporation in stishovite. *Phys. Chem. Mineras.* **33** (8-9), 613-621.

Bromiley G., Hilairet N. and McCammon, C. (2004a) Solubility of hydrogen and ferric iron in rutile and TiO_2 (II): Implications for phase assemblages during ultrahigh-pressure metamorphism and for the stability of silica polymorphs in the lower mantle. *Geophys. Res. Lett..* **31**, L04610.

Bromiley G., Keppler H., McCammon C., Bromiley F. and Jacobsen S. (2004b) Hydrogen solubility and speciation in natural, gem-quality Cr-diopside. *Am.. Mineral.* **89**, 941-949.

Donlon W.T., Mitchell T.E. and Heuer A.H. (1982) Precipitation in non-stoichiometric spinel. *J. Mat. Sci.* **17**, 1389-1397

Fukatsu N., Kurita N., Shiga H., Murai Y. and Ohashi, T. (2002) Incorporation of hydrogen into magnesium aluminate spinel. *Solid State Ionics* **152-153**, 809-817.

Gaetani G. and Grove T. (1998) The influence of water on melting of mantle peridotite. *Contrib. Mineral. Petrol.* **131**, 323-346.

Gonzalez R., Chen Y., Barhorst J. and Tsang, K. (1987) Protons and deuterons in stoichiometric and nonstoichiometric $MgAl_2O_4$. *J. Mat. Res.* **2** (1), 77-81.

Halmer M. (2006) Limitations of FTIR spectroscopy for detection of water in spinel group minerals when $^{IV}Fe^{2+}$ is incorporated into the crystal structure. *Spect. Lett.* **39**, 181-186.

Hertweck B., and Ingrin J. (2005) Hydrogen incorporation in a ringwoodite analogue: Mg_2GeO_4. *Mineral. Mag.* **69** (3), 337-343.

Huang X., Xu Y., and Karato S. (2005) Water content in the transition zone from electrical conductivity of wadsleyite and ringwoodite. *Nature* **434**, 746-749.

Ingrin J., and Skogby H. (2000) Hydrogen in nominally anhydrous upper-mantle minerals: concentration levels and implications. *Eur. J. Mineral.* **12**, 543-570.

Keppler H., and Bolfan-Casanova N. (2008) Thermodynamics of water solubility and partitioning. In *Water in nominally anhydrous minerals* (eds. H. Keppler and J. Smyth). Reviews in Mineralogy and Geochemistry, 62. Geochemical Society and Mineralogical Society of America. pp. 193-230

Kohlstedt D.L., Keppler H., and Rubie D. (1996) Solubility of water in the alpha, beta and gamma phases of $(Mg,Fe)SiO_4$. *Contrib. Mineral. Petrol.* **123**, 345-357.

Kohlstedt D.L. and Mackwell S.J. (1999) Solubility and diffusion of ‘water’ in silicate minerals. In: Catlow R. (ed.) *Microscopic properties and processes in minerals*. Kluwer, Dordrecht, 539-559.

Kröger F., and Vink H. (1956) Relations between the concentrations of imperfections in crystalline solids. In *Solid state physics: advances and applications* (eds. F. Seitz and D. Turnball). New York. pp. 307-435

Kudoh Y., Kuribayashi T., Mizohata H. and Ohtani E. (2000) Structure and cation disorder of hydrous ringwoodite, γ-$Mg_{1.89}Si_{0.97}O_4$. *Phys. Chem. Minerals* **27**, 474-479.

Lager G. and VonDreele R. (1996) Neutron powder diffraction study of hydrogarnet to 9.0 GPa. *Am. Mineral.* **81** (9-10), 1097-1104.

Lenaz D., Skogby H., Nestola F. and Princivalle F. (2008) OH incorporation in nearly pure $MgAl_2O_4$ natural and synthetic spinels. *Geochim. Cosmochim. Acta* **72**, 475-479.

Libowitzky E. (1999) Correlation of O-H stretching frequencies and O-H···O hydrogen bond lengths in minerals. *Monats. Chem.* **130** (8), 1047-1059.

Liermann H. and Ganguly J. (2002) Diffusion kinetics of Fe^{2+} and Mg in aluminous spinel: experimental determination and applications. *Geochim. Cosmochim. Acta* **66** (16), 2903-2913.

Lu R. and Keppler H. (1997) Water solubility in pyrope to 100 kbar. *Contrib. Mineral. Petrol.* **129**, 35-42.

Mackwell S., Kohlstedt D. (1990) Diffusion of hydrogen in olivine –implications for water in the mantle. *J. Geophys. Res.* **95** (B4) 5079-5088.

Mackwell S., Kohlstedt D. and Paterson M. (1985) The role of water in the deformation of olivine single crystals. *J. Geophys. Res.* **90** 11319-11333.

Martignago F., Dal Negro A., and Carbonin S. (2003) How Cr^{3+} and Fe^{3+} affect Mg-Al order-disorder transformation at high temperature in natural spinels. *Phys. Chem. Minerals* **30**, 401-408.

Meducin F., Redfern S., Le Godec Y., Stone H., Tucker M., Dove M. and Marshall W. (2004) Study of cation order-disorder in $MgAl_2O_4$ spinel by in situ neutron diffraction up to 1600 K and 3.2 GPa. *Am. Mineral.* **89**, 981-986.

Mitchell T. (1999) Dislocations and mechanical properties of MgO-Al_2O_3 spinel single crystals. *J. Am. Ceram. Soc.* **82**(12), 3305-16.

Nakamoto K., Margoshes M. and Rundle R. (1955) Stretching frequencies as a function of distances in hydrogen bonds. *J. Am. Chem. Soc.* **77**, 6480-6486.

Nestola F., Secco L., Bruno M., Prencipe M., Martignago F., Princivalle F. and Dal Negro A. (2009a) The effect of non-stoichiometry on high-temperature behaviour of $MgAl_2O_4$. *Mineral. Mag.* **73** (2), 301-306.

Nestola F., Smyth J., Parisatto M., Secco L., Princivalle F., Bruno M., Prencipe M. and Dal Negro A. (2009b) Effects of non-stoichiometry on the spinel structure at high-pressure: implications for Earth's mantle mineralogy. *Geochim. Cosmochim. Acta* **73** (2), 489-492.

Okamoto K. and Maruyama S. (2004) The eclogite-garnetite transformation in the MORB + H_2O system. *Phys. Earth Planet. Inter.* **146**, 283-296.

Okuyama Y., Kurita N., and Fukatsu N. (2006) Defect structure of alumina-rich nonstoichiometric magnesium aluminate spinel. *Solid State Ionics* **177**, 59-64.

Paterson M. (1982) The determination of hydroxyl by infrared absorption in quartz, silicate glasses and similar materials. *Bull. Mineral.* **105**, 20-29.

Rauch M. and Keppler H (2002) Water solubility in orthopyroxene. *Contrib. Mineral. Petrol.* **143**. 525-536.

Reddy K. and Cooper A. (1981) Oxygen diffusion in magnesium aluminate spinel. *J. Am. Ceram. Soc.* **64** (6), 368-371.

Redfern S., Harrison R., O'Neill H.S.C. and Wood D. (1999) Thermodynamics and kinetics of cation ordering in $MgAl_2O_4$ spinel up to 1600^oC from in situ neutron diffraction. *Am. Mineral*. **84**, 299-310.

Rossman G. and Smyth J. (1990) Hydroxyl contents of accessory minerals in mantle eclogites and related rocks. *Am. Mineral.* **75**, 775-780.

Saalfeld H. and Jagodzinski H. (1957) Segregation of Mg-Al spinels with an excess of Al_2O_3. *Z. Kris.* **109**, 87-109.

Shannon R. (1976) Revsied effective ionic radii and systematic studies of interatomic distances in halides and chaleogenides. *Acta Crystal. A* **32**, 751-767.

Sheldrick G. (1997) SHELX-97-a program for crystal structure refinement. Institut fur Anorganische Chemie, University of Gottingen, Germany.

Skogby H. (1994) OH incorporation in synthetic clinopyroxene. *American Mineralogist* **79** (3-4), 240-249.

Smyth J., Bell D. and Rossman G. (1991) Incorporation of hydroxyl in upper-mantle clinopyroxenes. *Nature* **351**, 732-735.

Smyth J., Holl C., Frost D., Jacobsen S., Langenhorst F. and McCammon C. (2003) Structural systematics of hydrous ringwoodite and water in Earth's interior. *Am. Mineral.* **88**, 1402-1407.

Smyth J., Holl C., Frost D. and Jacobsen S. (2004) High pressure crystal chemistry of hydrous ringwoodite and water in the Earth's interior. *Phys. Earth Planet. Inter.* **143-144**, 271-278.

Smyth J., Frost D., Nestola F., Holl C. and Bromiley G. (2006) Olivine hydration in the deep upper mantle: Effects of temperature and silica activity. *Geophys. Res. Lett.* **33**, L15301.

Stalder R. and Skogby H. (2003) Hydrogen diffusion in natural and synthetic orthopyroxene. *Phys. Chem. Mineral.* **30**, 12-19.

Stoe and Cie (1999) Crystal optimisation for numerical absorption correction. Stoe and Cie GmbH, Darmstad, Germany.

Thomas S.M., Koch-Muller M., Kahlenberg V., Thomas R., Rhede D., Wirth R. and Wunder, B. (2008) Protonation in germanium equivalents of ringwoodite, anhydrous phase B, and superhydrous phase B. *Am. Mineral.* **93** (8-9), 1282-1294.

Viertel H.U. and Seifert F. (1979) Physical properties of defect spinels in the system $MgAl_2O_4$-Al_2O_3. *N. Jb. Min. Abh.* **134**, 167-182.

Wang C. (1969) Growth and characterization of spinel single crystals for substrate use in integrated electronics. *J. App. Phys.* **40** (9), 3433-3444.

Warren M.C., Dove M.T. and Redfern S.A.T. (2000) Ab initio simulations of cation ordering in oxides: application to spinel. *J. Phys. Cond. Matter.* **12**, L43-L48.